16th ICAAR LISBOA 2020-2022

16th International Conference on
Alkali-Aggregate Reaction in Concrete
Lisboa | LNEC | Portugal | 31 May - 2 June 2022

http://icaar2020-2022.lnec.pt

A probabilistic homogenization approach for the computation of stiffness degradation in ASR-affected concrete

Thuc Nhu Nguyen [(1)], Emre Erkmen [(2)], Leandro F.M. Sanchez [(3)], Jianchun Li [(4)]

(1) University of Technology Sydney, Sydney, Australia; email: thucnhu.nguyen@student.uts.edu.au

(2) Concordia University, Montréal, Canada; email: emre.erkmen@concordia.ca

(3) University of Ottawa, Ottawa, ON, Canada; email: leandro.sanchez@uottawa.ca

(4) University of Technology Sydney, Sydney, Australia; email: jianchun.li@uts.edu.au

Abstract

There is a lack of effective and efficient approaches in current practices to evaluate in-situ condition of alkali-silica reaction (ASR) affected concrete structures, including their serviceability, load-carrying capacity, and residual strength, which jeopardises timely rehabilitation and leads to unnecessary risk and economic losses. In this context, numerical models are necessary to describe ASR-induced expansion and deterioration, enabling further analysis of ASR structural implications and providing critical information for a better decision making. This study proposes a probabilistic computational homogenization approach to describe the impact of ASR-induced meso-scale cracking on concrete stiffness. A Representative Volume Element (RVE) of concrete is created at the meso-scale level in which the Extended Finite Element Method is used for the implementation of ASR cracks and the interfacial transition zone (ITZ) to the damaged material. Uncertainty of model inputs such as aggregate and crack size and distribution are accounted for by utilizing a random generating algorithm. The reductions in the effective stiffness properties and the variations in results are then compared with experimental data. Results indicate a significant effect of ASR cracks distribution on the RVE stiffness and show the effectiveness of the RVE model in capturing the variation of stiffness reduction due to ASR.

***Keywords**: alkali-silica reaction; computational homogenization; crack configuration; probabilistic simulation; representative volume element*

1. INTRODUCTION

Alkali-silica reaction (ASR) is one of the most harmful distress mechanisms affecting the serviceability and durability of concrete infrastructure worldwide. Several approaches, recommendations, and test procedures, have been developed to assess the potential alkali-reactivity of concrete aggregates and the efficiency of preventive measures (e.g. control of the cement & concrete alkali content, use of supplementary cementing materials (SCMs), use of lithium-based admixtures, etc.) before their use in the field [1-4]. Despite a few issues with some of these test procedures and the constant need of improvement in the different standards/protocols, the majority of experts agree that in general, it is now possible to build new concrete infrastructure with limited risk of ASR. However, there is currently no consensus about the most efficient method(s) that should be implemented, and when, for the rehabilitation of ASR-affected concrete infrastructure [1, 5-7]. In this context, numerical models might be necessary, enabling further analysis of ASR structural implications and ensuring a better decision making.

The development of cracks within the aggregate particles at the early stages of the chemical reaction has been confirmed by a series of microscopic analyses from Sanchez et al [8, 9] through the *Damage Rating Index (DRI)* method. In order to capture the distress and damage development mechanisms due to ASR, Comby-Peyrot [10], Dunant and Scrivener [11], Cusatis et al [12], Ishakov et al [13], and Rezaghani et al [14] used meso-scale modeling. Meso-scale models generally introduce the aggregates and the cement paste explicitly; thus, concrete is modelled as a heterogeneous material with the aim of better understanding the effects of composite interactions and local damage mechanisms. Based on experimental observations, Sanchez et al [9] proposed a qualitative description of ASR induced crack generation and propagation as a function of its induced expansion development. A meso-scale computational model is required for the concrete material to adopt the qualitative model developed by Sanchez [9].

This work aims at developing a probabilistic meso-scale model to provide a thorough understanding of stiffness reduction as a function of ASR physicochemical development with consideration of uncertainty related to aggregates and cracks distribution. The crack pattern and extent from experimental observations are explicitly and efficiently established in the meso-scale model using the Extended Finite Element Method in a first-order computational homogenization framework. A random algorithm is utilized in generating aggregates and cracks into homogenized Representative Volume Elements. Finally, the numerical result is validated by experimental data and uncertainties due to the model inputs are quantified.

2. COMPUTATIONAL HOMOGENIZATION APPROACH

2.1.1 Equilibrium of a deformable body

The stress field is assumed continuous (before discretization), however, the displacement field is discontinuous between the interfaces. Let σ_{ij} denote the stress tensor and u_i be the displacement vector field, $\{u_i\} = \langle u_1\ u_2 \rangle^T = \boldsymbol{u}$. The stress tensor is related to the displacement gradient through the constitutive relation, i.e.

$$\sigma_{ij} = D_{ijkl} \frac{\partial u_k}{\partial x_l} \tag{1}$$

where components of the stiffness matrix D_{ijkl} , in general, are functions of the location vector $\{u_i\} = \langle u_1\ u_2 \rangle^T = \boldsymbol{u}$ in a heterogeneous continuum. We limit our analysis to 2D problems, therefore, all indices *i*, *j*, *k* and *l* vary between 1 and 2 throughout the manuscript and thus, the stiffness matrix for the bulk of the continuum generally has six independent components considering the symmetry of the shear stresses $\sigma_{12} = \sigma_{21}$, i.e.,

$$D = [D_{ij}] = \begin{bmatrix} D_{1111} & D_{1122} & D_{1112} \\ D_{1122} & D_{2222} & D_{2212} \\ D_{1112} & D_{2212} & D_{1212} \end{bmatrix} \tag{2}$$

The equilibrium equations can be written as

$$\frac{\partial \sigma_{ij}}{\partial x_j} + p_i = 0 \quad \text{in} \quad \Omega \tag{3}$$

$$u_i = r_i \quad \text{in} \quad \Gamma_D \tag{4}$$

$$\sigma_{ji} n_i = -s_j \quad \text{in} \quad \Gamma_N \tag{5}$$

where Ω, Γ and Γ_N are the analysis domain, Dirichlet and Neumann boundaries respectively, and n_i is the normal vector component to the boundary surface. Dirichlet and Neumann boundaries are non-overlapping and decompose the whole external boundary, i.e., $\partial\Omega = \Gamma$ where $\Gamma = \Gamma_D \cup \Gamma_N$ and $\Gamma_D \cap \Gamma_N = \emptyset$. The body force per unit volume in the analysis domain is denoted with p_i, the specified displacement at the Dirichlet boundary is r_i and the specified traction at the Neumann boundary is s_i. The Galerkin weak form of the above governing equations from Eqs. (3) to (5) can be expressed after integration by parts as

$$\int_\Omega \delta \frac{\partial u_j}{\partial x_i} \sigma_{ij} d\Omega + \int_\Omega \partial u_i p_i d\Omega + \int_{\Gamma_N} \partial u_i s_i d\Gamma = 0 \tag{6}$$

where the admissible displacement field u_i is prescribed at the boundary Γ_D as in Eq. (4) and therefore, its variation vanishes, i.e., $\partial u_i = 0$ in Γ_D.

2.1.2 Separation of scales and first-order homogenization

In the description of our problem, the assumption is that the heterogeneous medium has rapidly oscillating properties and the sizes of the heterogeneities are small compared to the overall size of the medium. Our aim is to compute the macro stiffness properties from the known meso-scale properties which represent an average and thus, the small-scale variations will not be present in the homogenized problem, i.e.,

$$\widehat{D}_{ijkl} \frac{\partial^2 \overline{u}_i}{\partial x_j \partial x_k} = -p_l \quad \text{in} \quad \Omega \tag{7}$$

where $\widehat{D}_{ijkl}$ are the components effective stiffness matrix after homogenization. In order to capture the meso-scale influence on the effective stiffness, a scaling parameter $\eta \to 1$ is introduced which represents the ratio between the size of the meso-scale structure and the macro-structure and thus, the

stiffness is assumed to be varying based on this small parameter [15]. Analytically, the homogenized stiffness $\hat{D}_{ijkl}$ is defined as the case when $\eta \to 0$. Therefore, the size of the heterogeneity is introduced as a variable to be able to describe the homogenous case as a special case, as shown in Figure 2.1.

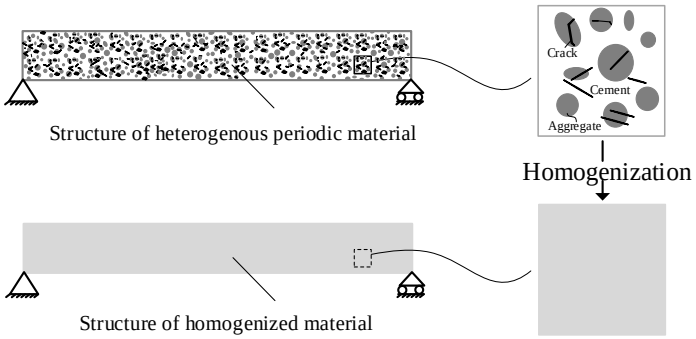

Figure 2.1: Schematic description of two-scale modelling based on homogenized material

The displacement field $\bar{u}_i$ in Eq. (7) is called the first approximate solution. The idea is to approximate the solution of the heterogeneous problem by using the solution of a simpler problem, which is the homogenous problem. Thus, $\bar{u}_i$ refers to the solution of a simpler homogenized problem and the complete displacement field $\bar{u}_i$ is represented in the form of asymptotic expansion as

$$u_i(\mathbf{x},\mathbf{y}) = \bar{u}_i(\mathbf{x},\mathbf{y}) + \eta\bar{\bar{u}}_i(\mathbf{x},\mathbf{y}) + \eta^2\bar{\bar{\bar{u}}}_i(\mathbf{x},\mathbf{y}) + \cdots \quad (8)$$

The oscillatory behaviour is due to heterogeneity and therefore, meso-scale oscillations are due to the higher-order contributions, i.e. $\bar{\bar{u}}_i$, $\bar{\bar{\bar{u}}}_i$,.... Due to different orders of η, that form of approximation in Eq. (8) introduces a hierarchy between the contributions of each term in the series. In order to make the position vector x_i independent of the scaling parameter η and thus, to construct globally valid solutions for a variable η, two spatial scales are incorporated into the problem. This allows x_i always refer to the same material point as η changes and the position vector x_i now has the meaning of the slow scale or the macro-scale coordinate, measuring variations within the global region of interest only. Therefore, in Eq. (8) there is another vector $y_i = x_i/\eta$ which is the fast coordinate, measuring variations within one period cell. As a result, the derivative operations transform into **[15]**

$$\frac{\partial}{\partial x_i} \to \frac{\partial}{\partial x_i} + \frac{1}{\eta}\frac{\partial}{\partial y_i} \quad (9)$$

Thus, the analysis domain of the problem is extended as $\Omega^\eta = \Omega \times \eta\mathrm{Y}$, where Y denotes the domain of one cell that periodically repeats. In this case, Eq. (3) takes the form

$$\frac{\partial \sigma_{ij}(\mathbf{x},\mathbf{y})}{\partial x_j} + \frac{1}{\eta}\frac{\partial \sigma_{ij}(\mathbf{x},\mathbf{y})}{\partial y_j} = -p_i(\mathbf{x}) \quad (10)$$

Where the asymptotic expansion of the stress tensor can be written as

$$\sigma_{ij}(\mathbf{x},\mathbf{y}) = \tilde{\sigma}_{ij}(\mathbf{x},\mathbf{y}) + \eta\tilde{\bar{\sigma}}_{ij}(\mathbf{x},\mathbf{y}) + \eta^2\tilde{\bar{\bar{\sigma}}}_{ij}(\mathbf{x},\mathbf{y}) + \ldots \quad (11)$$

By substituting Eq. (8) into Eq. (1) and using derivative transform in Eq. (9), one obtains

$$\bar{\sigma}_{ij}(\mathbf{x},\mathbf{y}) = D_{ijkl}(\mathbf{x},\mathbf{y})\left(\frac{\partial \bar{u}_k(\mathbf{x})}{\partial y_l}\right) \quad (12)$$

$$\tilde{\sigma}_{ij}(\mathbf{x},\mathbf{y}) = D_{ijkl}(\mathbf{x},\mathbf{y})\left(\frac{\partial \bar{u}_k(\mathbf{x})}{\partial x_l} + \frac{\partial \bar{\bar{u}}_k(\mathbf{x},\mathbf{y})}{\partial y_l}\right) = \bar{\sigma}_{ij}(\mathbf{x},\mathbf{y}) + \bar{\bar{\sigma}}_{ij}(\mathbf{x},\mathbf{y}) \quad (13)$$

$$\tilde{\bar{\sigma}}_{ij}(\mathbf{x},\mathbf{y}) = D_{ijkl}(\mathbf{x},\mathbf{y})\left(\frac{\partial \bar{\bar{u}}_k(\mathbf{x},\mathbf{y})}{\partial x_l} + \frac{\partial \bar{\bar{\bar{u}}}_k(\mathbf{x},\mathbf{y})}{\partial y_l}\right) \quad (14)$$

Because of the fact that the series in Eq. (11) does not contain the term $\eta^{-1}\breve{\sigma}_{ij}(\mathbf{x},\mathbf{y})$, Eq. (12) should vanish. This is because η^{-1} is not bounded as $\eta \to 0$ which is contrary to the periodicity assumption for $\sigma_{ij}(\mathbf{x},\mathbf{y})$. Thus, from Eq. (12) it can be concluded that $\overline{u}_i$ cannot depend on the fast coordinate **y**, i.e., $\overline{u}_i = \overline{u}_i(\mathbf{x})$. In the following analysis, only the first non-vanishing stress term is used, i.e., $\sigma_{ij}(\mathbf{x},\mathbf{y}) = \tilde{\sigma}_{ij}(\mathbf{x},\mathbf{y})$ and consequently, the terms higher than first order in the displacement ansatz are neglected, i.e., $\tilde{\tilde{\sigma}}_{ij}(\mathbf{x},\mathbf{y}) = 0$ and $u_i(\mathbf{x},\mathbf{y}) = \overline{u}_i(\mathbf{x}) + \eta\overline{\overline{u}}_i(\mathbf{x},\mathbf{y})$. Note that $\overline{\overline{u}}_i(\mathbf{x},\mathbf{y})$ is a periodic function in Y, i.e. $\overline{\overline{u}}_i(\mathbf{x},\mathbf{y}) = \overline{\overline{u}}_i(\mathbf{x},\mathbf{y}+\mathbf{Y})$, where **Y** is the period in fast coordinate. By substituting Eq. (13) into Eq. (10) and grouping the terms according to their order, i.e., $O(1)$ and $O(1/\eta)$ one obtains

$$\frac{\partial \tilde{\sigma}_{ij}(\mathbf{x},\mathbf{y})}{\partial x_j} + p_i(\mathbf{x}) = 0 \qquad \text{in} \qquad \Omega \tag{15}$$

$$\frac{\partial \tilde{\sigma}_{ij}(\mathbf{x},\mathbf{y})}{\partial y_j} = 0 \qquad \text{in} \qquad \mathrm{Y} \tag{16}$$

2.1.3 Variational setting for homogenization

By integrating the balance in Eq. (15) over a domain of one cell and using the variation of the first approximate displacement field $\delta\overline{u}_i$, after integration by parts the weak form of the equilibrium equation can be obtained as

$$\int_\Omega \delta\frac{\partial \overline{u}_j}{\partial x_i}\hat{\sigma}_{ij}\,\mathrm{d}\Omega + \int_\Omega \delta\overline{u}_i\, p_i\,\mathrm{d}\Omega + \int_{\Gamma_N} \delta\overline{u}_i\, s_i\,\mathrm{d}\Gamma = 0 \tag{17}$$

where $\hat{\sigma}_{ij}$ is the effective stress tensor and determined by averaging the stress tensor over one cell, i.e.

$$\hat{\sigma}_{ij} = |\mathrm{Y}|^{-1}\int_\mathrm{Y} \sigma_{ij}(\mathbf{x},\mathbf{y})\mathrm{dY} = |\mathrm{Y}|^{-1}\int_\mathrm{Y}\left[\bar{\sigma}_{ij}(\mathbf{x},\mathbf{y}) + \overline{\overline{\sigma}}_{ij}(\mathbf{x},\mathbf{y})\right]\mathrm{dY} \tag{18}$$

where $|\mathrm{Y}| = \int_\mathrm{Y}\mathrm{dY}$ is the area of the cell (i.e. volume for unit thickness). In obtaining Eq. (17), it has been assumed that the source terms p_i and s_i are independent of the fast coordinate y_i. For the solution of the global equilibrium problem in Eq. (17), the whole stress tensor σ_{ij} needs to be expressed in terms of the average displacement gradient $\partial\overline{u}_i/\partial x_j$. For that purpose, Eq. (16) is used in the weak form by multiplying with the virtual displacement fluctuations $\delta\overline{\overline{u}}_i$ and integrating over a domain of one cell **Y**. After integration by parts with respect to fast coordinate y_i, one obtains

$$\int_\mathrm{Y} \delta\frac{\partial \overline{\overline{u}}_j}{\partial y_i}\sigma_{ij}\mathrm{dY} - \int_\Psi \delta\overline{\overline{u}}_j\,\sigma_{ji}n_i\mathrm{d}\Psi = 0 \tag{19}$$

where $\Psi = \partial\mathrm{Y}$ is the boundary of the cell and Ψ represents the fast coordinate on the cell boundary. Eq. (19) is the Hill-Mandel condition for scale separation, which allows decoupling of the analysis of a heterogeneous material into analyses at the local and global levels. Thus, the solution of Eq. (19) builds the relationship between the gradients of the average displacement and the stress in one cell Y. Under the assumption of $\eta \to 0$, by using Eq. (19), the weak form over the whole domain in Eq. (6) can be replaced with Eq. (17) for the global analysis. Thus, the heterogeneous domain can be replaced by the equivalent homogenous material having calculated the effective properties at the local level. Despite the fact that $\overline{\overline{u}}_i(\mathbf{x},\mathbf{y})$ is a periodic function, i.e., $\int_\mathrm{Y}\frac{\partial\overline{\overline{u}}_i(\mathbf{x},\mathbf{y})}{\partial y_j}\mathrm{dY} = \mathbf{0}$, the integral of the stress component $\overline{\overline{\sigma}}_{ij}$ generally does not vanish in Y, i.e., $\int_\mathrm{Y}\overline{\overline{\sigma}}_{ij}(\mathbf{x},\mathbf{y})\mathrm{dY} = \int_\mathrm{Y} D_{ijkl}(\mathbf{x},\mathbf{y})\frac{\partial\overline{\overline{u}}_k(\mathbf{x},\mathbf{y})}{\partial y_l}\mathrm{dY} \neq \mathbf{0}$ thus, the two-scale analysis introduces the effect of fluctuations due to heterogeneity in the global analysis.

2.1.4 RVE Boundary Value Problem

In order to solve the cell problem in Eq. (19) a Representative Volume Element (RVE) needs to be introduced. The RVE is defined as the smallest micro-structural volume that sufficiently accurately represents the overall macroscopic stiffness properties of interest. Thus, the size of the RVE should be selected large enough to be statistically representative of the distributions of the inclusions. Because of the finite size of the RVE, i.e., $\eta \neq 0$, homogenization is approximate unless exact RVE boundary conditions are imposed. Since exact boundary conditions are not known *a-priori* a chosen RVE is generally analysed using either uniform gradient, uniform traction or periodic boundary conditions. Therefore, the information on the cell boundary is lost due to Hill-Mandel condition for scale separation as there might be many candidates for $\eta\bar{\bar{u}}_i$ that satisfy Eq. (19). In other words, there is a micro-scale effect due to micro-fluctuations at the boundary of a finite size RVE that is not resolved in the two-scale analysis. The assumed micro-scale field existing at the RVE boundary influences the effective modulus by influencing the effective stress field, e.g. in Kanit et al. [16]. We assume that the aggregate and ASR induced crack distributions are such that the whole structure consists of spatially repeated cells as indicated in Figure 2.1. Therefore, Periodic Boundary Conditions are assumed herein and implemented to determine the average displacement field of the homogenized RVE.

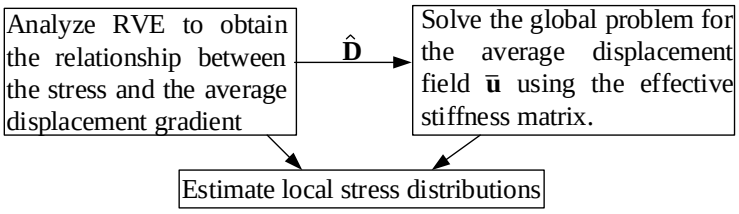

Figure 2.2: Schematic outline for the two-scale analysis procedure

The schematic outline in Fig. 2.2 describes the multi-scale analysis procedure based on the idea of separation of scales. Once the boundary conditions are chosen, equations can be solved to calculate the local RVE stress tensor σ_{ij} . Accordingly, the effective stress tensor $\hat{\sigma}_{ij}$ can be calculated by using the local stress tensor σ_{ij} in Eq. (18). Three cases of displacement gradient need to be introduced to determine all components of the stiffness matrix through the displacement gradient and stress relationship, i.e.

$$\begin{bmatrix} \hat{\sigma}_{11}^1 & \hat{\sigma}_{11}^2 & \hat{\sigma}_{11}^3 \\ \hat{\sigma}_{22} & \hat{\sigma}_{22}^2 & \hat{\sigma}_{22}^3 \\ \hat{\sigma}_{12} & \hat{\sigma}_{12}^2 & \hat{\sigma}_{12}^3 \end{bmatrix} = \begin{bmatrix} \hat{D}_{1111} & \hat{D}_{1122} & \hat{D}_{1112} \\ \hat{D}_{1122} & \hat{D}_{2222} & \hat{D}_{2212} \\ \hat{D}_{1112} & \hat{D}_{2212} & \hat{D}_{1212} \end{bmatrix} \begin{bmatrix} \overset{\text{Case1}}{1} & \overset{\text{Case2}}{0} & \overset{\text{Case3}}{0} \\ 0 & 1 & 0 \\ 0 & 0 & 1 \end{bmatrix} \tag{24}$$

It should be noted that the resulting stiffness matrix is symmetrical.

3. PROBABILISTIC MODEL FOR CONCRETE STIFFNESS REDUCTION DUE TO ASR

3.1 ASR distress development and its effect on concrete stiffness properties

ASR in concrete generates a secondary product (i.e. ASR gel) that induces pressure and leads to crack formation within the aggregate particles and surrounding cement paste, shown in **Figure 3.1**. Sanchez[23] proposed a qualitative meso-scale model to describe ASR cracks generation and propagation as a function of its induced expansion development. According to the author, ASR cracks are initially developed within aggregate particles at low expansion levels (i.e. up to 0.05%). At moderate levels of expansion (i.e. 0.12%), although some additional cracks are still generated within the aggregates, the existing cracks previously formed at low expansion levels keep propagating and may reach the boundaries of the aggregate particles. Once the expansion increases to higher levels (i.e. > 0.2%), the overall damage is mostly dominated by the propagation of pre-existing cracks to the surrounding cement paste. It is worth noting that two types of cracks may be induced by ASR in concrete: (1) cracks “cutting”

the aggregate particles, namely “sharp cracks” (type A), and (2) cracks outlining the aggregate particle boundaries, namely “onion skin cracks” (type B). The proportion of onion cracks (type B) seems to be about 20-30 % of the total cracks, yet it may vary according to the aggregate lithotype (i.e. mineralogy).

In the research conducted by Sanchez et al [9], crack density (count/cm^2) has been related to the reduction of stiffness of affected concrete. Figure 3.1(b) illustrates experimental observation from Sanchez et al [9] on crack densities corresponding to different levels of expansion reached by 35 MPa concrete specimens incorporating distinct reactive coarse aggregates. As the expansion level increases, the elasticity modulus reduces while the crack density increases. According to [8, 9], the proportion of open cracks in aggregate and cement paste are different for different concrete mixtures and levels of expansion. However, in all tested specimens, the majority of open cracks are found in the aggregate particles, being around 70% to 85% of the total number of cracks. More details on the experimental setup and measurements can be found in Sanchez et al [2, 8, 9].

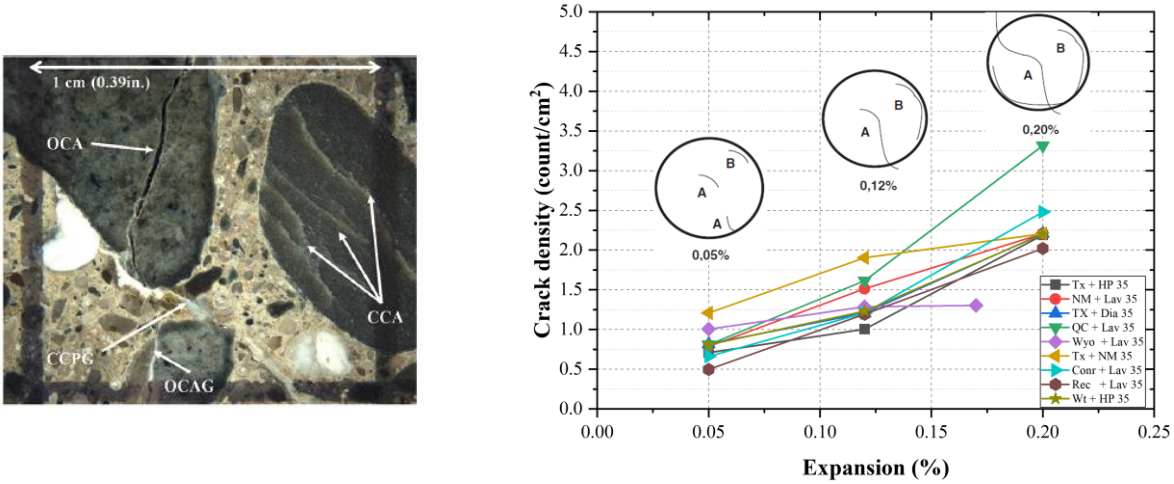

(a) (b)

Figure 3.1: Crack development due to ASR: (a) Open cracked in aggregate and cement paste; (b) Crack density with qualitative crack development model vs expansion degree measured and proposed by Sanchez et al [9]

3.2 Development of RVE with randomly distributed aggregates and ASR induced cracks

This part presents the process of developing two-phase homogenized RVE and introducing ASR cracks into the RVE. Radom algorithm is adopted in generating inner geometry of concrete and locating cracks (i.e. location and direction). The uncertainty due to differences in aggregate size/distribution and crack distribution, therefore, is evaluated.

3.2.1 RVE of concrete with random aggregates distribution

The proposed computational homogenization approach in the previous sections is utilised for modelling of elastic properties of ASR affected concrete. A two-phase Representative Volume Element (RVE) of the material at the mesoscale is constituted by aggregates and cement paste.

The take-and-place method proposed in [17] is adopted herein for aggregate generation and placement so that both aggregate particles size and their distribution are random. In this process, a typical aggregate size distribution curve is adopted and divided into segments, then the aggregate particles are randomly generated with assuming uniform probability distribution of the aggregate size in each segment. In the placing process, aggregate particles are randomly placed into the RVE model without intersection between the particles. This taking-and-placing process requires information of (1) aggregate size distribution, (2) shape of aggregates and (3) aggregate volume fraction. Without ASR damage, the volume fraction and properties of aggregates and cement paste determine the stiffness of the RVE, where the shape of aggregates has a little effect [18]. In this study, aggregate area fraction is considered instead of the aggregate volume fraction in 3D models. It’s worth noting that the aggregate volume fraction is always smaller than the aggregate area fraction and literature shows that the aggregate area fraction from 0.4 to 0.5 is reasonable in the 2D mesoscale model of concrete [19]. Therefore, the aggregate area faction is assumed to be 0.45 for all the RVE models in this study. In addition, Kim et al.

[18] shows that the shape of aggregates in meso-scale models of concrete has a little effect on its elastic behaviour. The circular aggregate shape is thus used in the RVE model for simplicity and minimising computational cost. The minimum and maximum aggregate particles diameter of 4.75 mm and 19.5 mm, respectively, is adopted as same as reported in the experimental testing of Sanchez et al [9]. The aggregate size distribution and typical RVE are shown in Figure 3.2.

As discussed by Mirkhalaf et al. [20] and Rezakhani et al. [21], size of RVE should be more than three times of the maximum aggregate size so that the RVE is a representative of the homogeneous concrete composite; yet, it is not too large with a high computational cost. In this study, 75 x 75 mm^2 RVE size is selected and deemed accurate. The number of 4-node square elements used is 1600, which is small enough to keep the computational cost reasonably low. Lines of discontinuity due to phase changes (from aggregate to cement paste) are introduced using the Extended Finite Element Method, while keeping the underlying mesh regular [22]. As the bond between aggregate particles and cement paste is assumed to be perfect, very large interface cohesive stiffness values are used to represent the bond. Before ASR occurrence, the area fraction and properties of aggregates and cement paste determine the stiffness of the RVE [23]. In this study, the elastic modulus of mortar and coarse aggregate are adopted as typical values, 20 GPa and 60 GPa, respectively, where Poisson's ratio of both materials are assumed to be the same value 0.2.

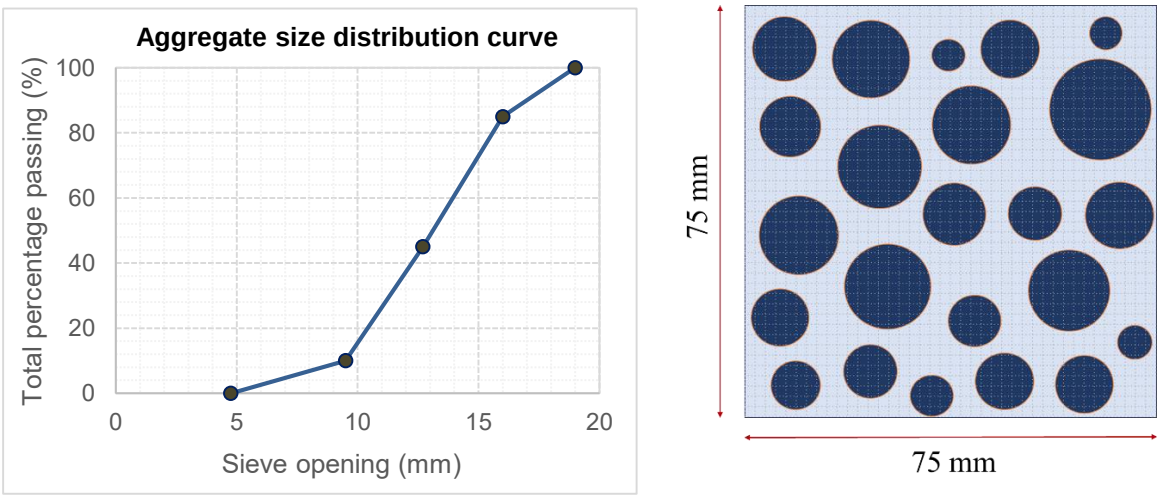

Figure 3.2: Aggregate size distribution and typical RVE with the random aggregate generation

3.2.2 RVE of ASR affected concrete with random cracks distribution

The stiffness of ASR affected concrete at three expansion levels of 0.05%, 0.12% and 0.2% are modelled using the proposed computational homogenization method by introducing different degrees of open cracks into the RVE that developed in the previous section. Open cracks were introduced into the RVE model by using the Extended Finite Element Method [24]. ASR induced cracks are assumed completely open, and therefore, the interface cohesive stiffness along the cracks is assumed as zero. It should be noted that the stiffness of the aggregates and cement paste are assumed to remain the same at different levels of expansion and thus, the change in the effective properties of the macro-scale concrete is only due to development of open cracks at the meso-scale.

Crack density in [9] obtained in count/cm^2 was converted to count/element to input to the RVE, while the location and development of the cracks were followed the qualitative damage model proposed in the same study. Three main types of cracks in ASR affected concrete with different proportions suggested in [9] are crack in cement paste, onion and shape cracks in aggregate. In this study, the proportion of cracks in cement paste is assumed to be 25% for all the RVE models, where the aggregate cracks consist of onion and shape crack of 40% and 60%, respectively. Onion cracks in the RVE model are considered to be parallel to the aggregate boundary at 75% of the aggregate radius. The extension of the crack is predefined based on the crack density corresponding to the ASR expansion level. For the selected mesh of 1600 elements, the onion cracks were extended to a total of 81, 125 and 198 number of elements for 0.05%, 0.12% and 0.20% expansion levels, respectively. The shape cracks occur inside randomly selected aggregates. Similarly, for the given mesh, shape cracks extend to a total of 122, 189

and 297 number of elements for 0.05%, 0.12% and 0.20% expansion levels, respectively. Inside the cement paste, cracks were introduced for a total of 68, 105 and 165 number of elements for 0.05%, 0.12% and 0.20% expansion levels, respectively. Details of cracks data for model inputs are presented in Table 3.1.

Table 3.1: Information on open cracks in the RVE of ASR affected concrete

Expansion level	Crack density (count/cm^2)	Crack density (count/mesh element)	Total length of crack in cement (count)	Total number of crack in aggregate (count)	Shape crack (count)	Onion crack (count)
0.05%	0.9	0.169	68	203	122	81
0.12%	1.4	0.263	105	315	189	126
0.20%	2.2	0.413	165	495	297	198

The stiffness of cracked concrete is affected by not only the number of open cracks in aggregate and cement paste presented previously but also their distribution. To quantify this variation, the starting point of cracks and their directions are randomly generated to quantify related uncertainties by an automatic process using the random algorithm. In this automatic process of crack generation, the shape crack in aggregate is restrained to extend inside of the aggregate before its length reaches the aggregate diameter value or expansion level reach 0.2%. Cracks initiated in cement paste remain in cement paste at all the expansion levels. In addition, the onion crack in aggregate keep extending parallel to aggregate boundary until reaching crack length limit but not getting a closed circle. Typical development of ARS cracks in a single aggregate is shown in Figure 3.3. Combination of random aggregate size/distribution and random location/direction of cracks in aggregate and cement paste, uncertainties related to these model input parameters are evaluated.

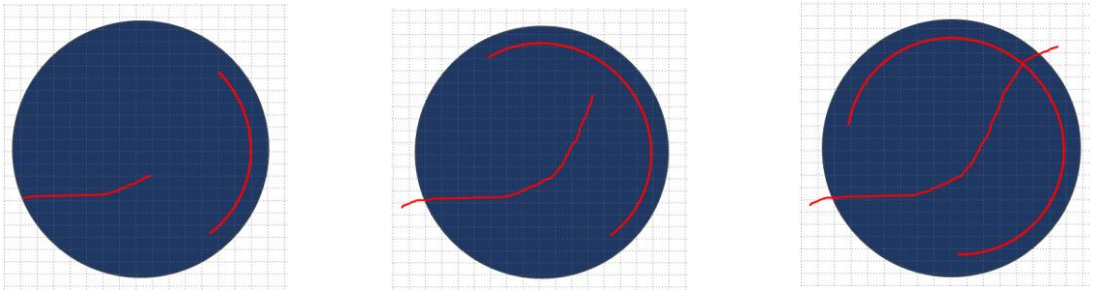

(a) 0.05% (b) 0.12% (c) 0.2%

Figure 3.3: Typical development of cracks in a single aggregate in the RVE

4. RESULTS AND DISCUSSION

The results of the RVE modelling are shown in Table 4.1 and plotted in Figure 4.1 against the experimental data from Sanchez at al [9] for 5 different mixtures of 35 MPa concrete. The results are collected from more than 30 RVE models with different aggregate and cracks distribution at each expansion level.

The effective stiffness of the concrete without ASR cracks is in a reasonable range, and variate in a small range when keeping the same aggregate volume fraction but changing the number, size and distribution of aggregates. For the ASR affected concrete model, introducing open cracks into the RVE model at the mesoscale significantly reduce its effective stiffness. The result shows that the stiffness reduces at a higher rate at lower expansion levels (i.e. up to 0.12%) which is commonly observed from many other experimental studies.

In comparison with the experimental result, the numerical simulation provides slightly lower stiffness reduction at all the expansion levels in term of mean values. This result could be due to either number of the available experimental data, or the reduction in elastic properties of aggregate, cement paste and their bond caused by micro-cracks that was not considered in this study. Further investigation needs to

be done by both means of experimental and numerical study. Still, all the experimental data are captured in the variation range of RVE effective stiffness. High ranges of variations are obtained from the RVE models at all the expansion levels as the cracks distribution changes. It shows a significant effect of open cracks distribution on the effective stiffness of the homogenized RVE.

Table 4.2: Effective stiffness properties of ASR affected concrete: Numerical vs experimental results

Expansion Level (%)	RVE model			Experiment [9]
	Effective stiffness (GPa) Mean [Min-Max]	Reduction Variation (%)	Reduction Mean (%)	Reduction Mean (%)
0.00%	39.7 [39.0 – 40.2]	-	-	-
0.05%	33.4 [27.3 – 37.6]	5.3 – 31.2	15.8	16.1%
0.12%	27.8 [19.4 – 32.6]	17.9 – 51.1	29.9	33.6%
0.20%	23.6 [15.9 – 29.3]	26.2 – 59.9	40.5	41.1%

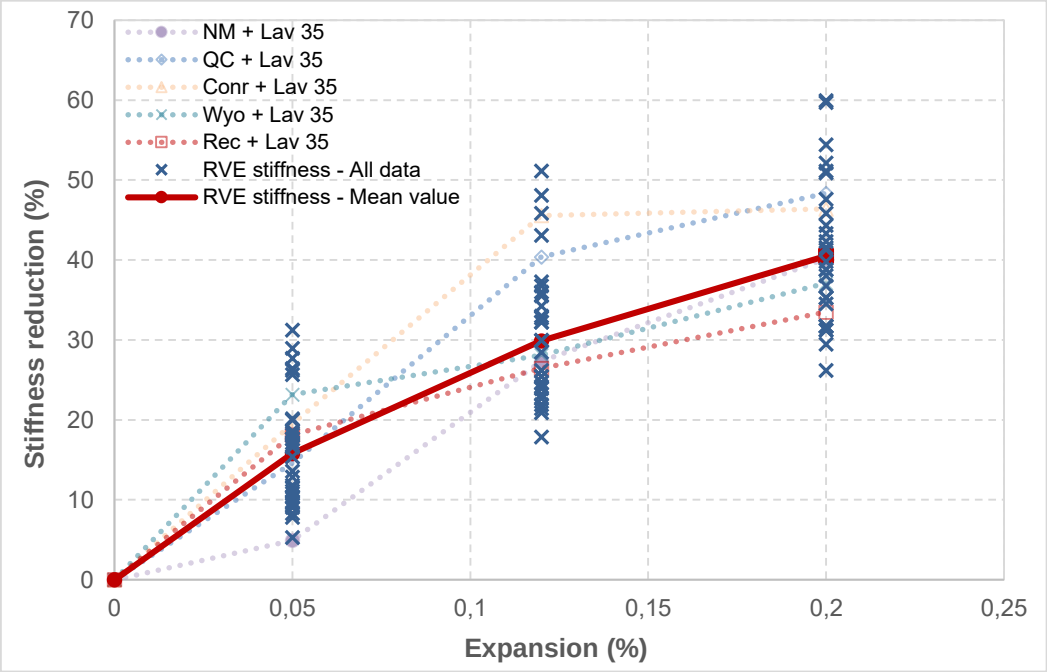

Figure 4.1: Reduction of concrete stiffness obtained from the homogenized RVE compared to experimental data

5. CONCLUSIONS

A probabilistic computational homogenization procedure was developed to determine the effective stiffness of ASR-affected concrete mixtures and take into account uncertainties regarding aggregates and cracks distribution. The meso-scale RVE model was continuum-based in which aggregates and cement matrix were assumed fully bonded in the concrete mix. ASR induced cracks were considered fully open, i.e., cohesionless and frictionless. Discontinuities (due to phase changes and/or crack openings) were efficiently introduced into the regularly meshed RVE model by using the Extended Finite Element Method. To consider uncertainties due to differences in aggregate size and cracks distribution, the aggregate and cracks were generated by a random algorithm. The effect of uncertainties of model

inputs are reported and the average values and deviations in numerical results show very good agreements with those of the experimental results of ASR affected 35 MPa concrete. The results show that randomness in the distribution of aggregates has a small effect on effective stiffness of the RVE models while the randomness in the distribution of open cracks produces significant stiffness variation.

With promising results, however, this probabilistic model still needs to be improved by considering uncertainties due to variations of crack density and constitutive material properties. In addition, it is also desirable to extend the probabilistic homogenization approach to higher expansion levels (i.e. > 0.2%) of ASR affected concrete.

6. ACKNOWLEDGMENTS

The authors wish to express their gratitude and sincere appreciation to the Mitacs Globalink Research Award, UTS FEIT HDR Collaboration Experience Award**,** the Australian Research Council Research Hub (IH150100006) for Nanoscience Based Construction Materials Manufacturing (NANOCOMM) and the industry partner Roads and Maritime Services (RMS) for financing this research.

7. REFERENCES

[1] Fournier, B.; Bérubé, A., “Alkali-aggregate reaction in concrete: a review of basic concepts and engineering implications”, *Canadian Journal of Civil Engineering*, 27, 2000, No. 2, pp. 167-191.

[2] Sanchez, L.F.M., “Contribution to the Assessment of Aging Concrete Infrastructures Affected by Alkali-Aggregate Reaction”, PhD Thesis, Université Laval, 2014.

[3] ASTM C 1293. “Standard test method for determination of length change of concrete due to alkali-silica reaction”. ASTM International, West Conshohocken (USA), 2012.

[4] AASHTO, “Determining the Reactivity of Concrete Aggregates and Selecting Appropriate Measures for Preventing Deleterious Expansion in New Concrete Construction: Final Report”, FHWA & AASHTO ASR Task Group, 2010.

[5] Folliard, K.J., Barborak, R., Drimalas, T., Du, L., Garber, S., Ideker, J., Ley, T., Williams, S., Juenger, M., Fournier, B., Thomas, M.D.A., "Preventing ASR/DEF in New Concrete: Final Report”, Texas Department of Transportation (TxDOT), 2006.

[6] Malvar, L.J., Cline, G.D., Burke, D.F., Rollings, R., Sherman, T., Greene J., “Alkali-Silica Reaction Mitigation: State-of-the-Art”, Final Report, Naval Facilities Engineering Service Center, 2001.

[7] Ballard, Zachoriah J., William S. Caires, and Stanley R. Peters, “Alternate Mitigation Materials for Alkali-Silica Reaction (ASR) in Concrete”, No. CDOT-2008-10. Colorado Department of Transportation, DTD Applied Research and Innovation Branch, 2008.

[8] Sanchez, L. F. M.; Fournier, B.; Jolin, M.; Bedoya, M. A. B.; Bastien, J., and Duchesne, J., “Use of Damage Rating Index to Quantify Alkali-Silica Reaction Damage in Concrete: Fine versus Coarse Aggregate,” ACI Materials Journal, V. 113, 2016, No. 4, pp. 395–407.

[9] Sanchez, L. F. M.; Fournier, B.; Jolin, M., and Duchesne, J., “Reliable quantification of AAR damage through assessment of the Damage Rating Index (DRI), “Cement and Concrete Research,” V. 67, 2015, pp. 74-92.

[10] Comby-Peyrot, I.; Bernard, F.; Bouchard, P.O.; Bay, F., and Garcia-Diaz, E., “Development and validation of a 3D computational tool to describe concrete behaviour at mesoscale. Application to the alkali-silica reaction,” Computational Material Science, V. 46, 2009, pp. 1163-1177.

[11] Dunant, C.F., and Scrivener, K.L., “Micro-mechanical modelling of alkali-silica reaction induced degradation using AMIE framework,” Cement and Concrete Research, V. 40, 2010, pp. 517-525.

[12] Cusatis, G.; Di Luzio, G., and Cedolin, L., “Meso-scale simulation of concrete: Blast and Penetration affects and AAR degradation,” Applied Mechanics and Materials, V. 82, 2011, pp. 75-80.

[13] Ishakov, T.; Timothy, J.T., and Meschke, G., “Expansion and deterioration of Concrete due to ASR: Mechanical Modelling and Analysis,” Cement and Concrete Research, V.115, 2019, pp. 507-518.

[14] Rezaghani, R., Alnaggar, M., and Cusatis, G., “Multiscale homogenization analysis of Alkali-Silica Reaction (ASR) Effect in Concrete,” Engineering, 2019.

[15] Holmes, M.H. Introduction to Perturbation Methods, 2013, 2nd edition, Springer.

[16] Kanit, T.; Forest, S.; Galliet, I.; Mounoury, V., and Jeulin, D., “Determination of the size of the representative volume element for random composites: statistical and numerical approach,” *International Journal of Solids and Structures*, V. 40, 2003, pp. 3647-3679.

[17] Wang, Z.M., Kwan, A.K.H. and Chan, H.C, Mesoscopic study of concrete I: generation of random aggregate structure and finite element mesh. Computers & structures, v70, 1999, pp.533-544.

[18] Kim, S. M., and Al-Rub, R. K. A., “Meso-scale computational modeling of the plastic-damage response of cementitious composites,” Cement and Concrete Research, V. 41, 2011, No.3, pp. 339-358.

[19] Zheng, J.J., Mesostructure of concrete-stereological analysis and some mechanical implications, Delft University, The Netherlands, 2000.

[20] Mirkhalaf, S. M.; Pires, F. A., and Simoes, R., “Determination of the size of the Representative Volume Element for the simulation of heterogeneous polymers at finite strains,” Finite Elements in Analysis and Design, V.119, 2016, pp. 30-44.

[21] Rezakhani, R.; Zhou, X., and Cusatis, G., “Adaptive multiscale homogenization of the lattice discrete particle model for the analysis of damage and fracture in concrete,” International Journal of Solids and Structures, V.125, 2017, pp.50-67.

[22] Sukumar, N.; Chopp, D.L.; Moes, N., and Belytschko, T. C., “Modeling voids and inclusions by level sets in extended finite element method,” Computer Methods in Applied Mechanics and Engineering, V. 190, 2001, pp. 6183-6200.

[23] Wriggers, P., and Moftah, S.O., “Mesoscale models for concrete: Homogenisation and damage behavior,” Finite Elements in Analysis and Design, V. 42, 2006, No. 7, pp.623-636.

[24] Belytschko, T., and Black, N., “Elastic crack growth in finite elements with minimal remeshing,” International Journal for Numerical Methods in Engineering, V.45, 1999, pp. 601-620.